SCIENCE CHINA
Earth Sciences

•REVIEW•

January 2024 Vol.67 No.1: 61–78
https://doi.org/10.1007/s11430-022-1218-0

Impacts of major volcanic eruptions over the past two millennia on both global and Chinese climates: A review

Weiyi SUN[1], Deliang CHEN[2], Guonian LÜ[1], Liang NING[1], Chaochao GAO[3], Renhe ZHANG[4], Bin WANG[5] & Jian LIU[1,6,7*]

[1] *Key Laboratory for Virtual Geographic Environment, Ministry of Education; State Key Laboratory Cultivation Base of Geographical Environment Evolution of Jiangsu Province; Jiangsu Center for Collaborative Innovation in Geographical Information Resource Development and Application; School of Geography Science, Nanjing Normal University, Nanjing 210023, China;*
[2] *Regional Climate Group, Department of Earth Sciences, University of Gothenburg, Gothenburg 40530, Sweden;*
[3] *College of Environmental and Resource Science, Zhejiang University, Hangzhou 310058, China;*
[4] *Department of Atmospheric and Oceanic Sciences & Institute of Atmospheric Sciences, Fudan University, Shanghai 200437, China;*
[5] *Department of Atmospheric Sciences and Atmosphere-Ocean Research Center, University of Hawaii at Manoa, Honolulu, HI 96825, USA;*
[6] *Jiangsu Provincial Key Laboratory for Numerical Simulation of Large Scale Complex Systems, School of Mathematical Science, Nanjing Normal University, Nanjing 210023, China;*
[7] *Open Studio for the Simulation of Ocean-Climate-Isotope, Qingdao National Laboratory for Marine Science and Technology, Qingdao 266237, China*

Received November 28, 2022; revised August 29, 2023; accepted October 31, 2023; published online December 6, 2023

Abstract Major volcanic eruptions (MVEs) have attracted increasing attention from the scientific community. Previous studies have explored the climatic impact of MVEs over the past two millennia. However, proxy-based reconstructions and climate model simulations indicate divergent responses of global and China's regional climates to MVEs. Here, we used multiple data from observations, reconstructions, simulations, and assimilations to summarize the historical facts of MVEs, the characteristics and mechanisms of their climatic impact, and directions for future research. We reviewed volcanic datasets and determined intensive MVE periods; these periods corresponded to the years 530–700, 1200–1460, and 1600–1840 CE. After tropical MVEs, a substantial cooling effect is observed throughout the globe and China on the interannual-interdecadal time scales but an inconsistent cooling magnitude is detected between reconstructions and simulations. In the first summer after tropical MVEs, a decrease in global and monsoonal precipitation is observed. In reconstructions and simulations, an increased precipitation is seen for the Yangtze River Basin, while large uncertainties in precipitation changes are present for other regions of China. Decadal drought can be induced by frequent eruptions and volcanism superimposed on low solar irradiation and internal variability. MVEs affect climate directly through the radiative effect and indirectly by modulating internal variability, such as the El Niño–Southern Oscillation (ENSO) and Atlantic Multidecadal Oscillation (AMO). However, changes in the phase, amplitude, and periodicity of ENSO and AMO after MVEs and the associated mechanisms remain controversial, which could account for model-reconstruction disagreements. Moreover, other internal variability, uncertainties in reconstruction methods and aerosol–climate models, and climate background may also induce model-reconstruction disagreements. Knowledge gaps and directions for future research are also discussed.

Keywords Major volcanic eruption, Climate variability, Mechanism, Past two millennia, Internal variability

Citation: Sun W, Chen D, Lü G, Ning L, Gao C, Zhang R, Wang B, Liu J. 2024. Impacts of major volcanic eruptions over the past two millennia on both global and Chinese climates: A review. Science China Earth Sciences, 67(1): 61–78, https://doi.org/10.1007/s11430-022-1218-0

* Corresponding author (email: jliu@njnu.edu.cn)

1. Introduction

On January 15, 2022, a violent undersea volcano eruption at Hunga Tonga-Hunga Ha'apai (HTHH; 20.57°S, 175.38°W), an island country in the South Pacific, generated a strong earthquake and tsunami. A volcanic cloud was formed approximately 57 km above sea level (Proud et al., 2022), which discharged approximately 3.6 million tons of volcanic mineral particles and other substances into the atmosphere, forming global-scale atmospheric waves (Wright et al., 2022). In a manner that was distinct from other explosive eruptions, the HTHH erupted a large amount of water vapor into the stratosphere (Millán et al., 2022), accelerating the stratospheric aerosol formation (Zhu et al., 2022) and changing the Antarctic Ozone, consequently affecting Pacific sea surface temperature (SST) remotely (Hartmann, 2022). This eruption is considered to be the most violent volcanic eruption of the 21st century. The last strong volcanic eruption was the Pinatubo eruption on June 15, 1991, with an intensity of 6, as measured using the Volcanic Exploration Index (VEI). The HTHH had a VEI of 5 and was approximately 5.7% of the size of Pinatubo. In this study, volcanic eruptions with a VEI >6 are considered as major volcanic eruptions (MVEs). The climatic impact of potential MVEs is of great concern to the international community.

Volcanic eruptions are one of the most important external forcing factors for the global climate system. An eruption injects sulfate aerosols into the stratosphere, which are formed through the reaction between sulfur dioxide (SO_2) and hydroxide (OH) or water vapor (H_2O). The sulfate aerosols decrease with a typical e-folding time of approximately 12–14 months. Aerosols can perturb the global climate by scattering incoming solar radiation, resulting in global surface cooling that may last for 2–3 years (Robock, 2000). Recently, considerable progress has been made in analyzing the radiative effects of volcanic aerosols and determining the physics, microphysics, and chemistry of such processes (Zanchettin et al., 2016). The Model Inter-comparison Project on the climatic response to volcanic forcing (VolMIP) and the Interactive Stratospheric Aerosol Model Inter-comparison Project (ISA-MIP) have contributed to the sixth phase of the Coupled Model Intercomparison Project (CMIP6) (Zanchettin et al., 2016; Timmreck et al., 2018). These projects attempt to implement different climate models to simulate the volcanic impact on climate, constrain interactive stratospheric aerosol models, and reduce uncertainty in volcanic aerosol forcings. However, volcanic forcing and volcanic climate effects simulated by the CMIP5/6 models remain hindered by several uncertainties in its implementation (IPCC, 2021).

Instrumental data are available for a limited number of volcanic eruptions with small magnitudes; hence, the associated volcanic climate impact signals are quite noisy (Zanchettin et al., 2016). This necessitates a comprehensive review of volcanic activity over a sufficiently historical period (e.g., the past 2,000 years), ensuring a large sample size. For example, over the past 2,000 years, 27 MVEs with intensities exceeding that of the 1991 Pinatubo eruption have been recorded (Sigl et al., 2015). Meanwhile, because global warming causes a mean state change, further amplifying the climatic effect of volcanism, we compared differences in the impacts of volcanic eruptions on climate under cold and warm climate backgrounds (Fasullo et al., 2017).

As a core project of the International Geosphere-Biosphere Program (IGBP), Past Global Changes (PAGES) published its scientific plan for the next ten years in 2009, proposing to take the past 2,000 years as the main period to analyze climatic and environmental evolution. Considerable progress has been made in obtaining both climatic and volcanic reconstruction data, both of which provide opportunities for analyzing the volcanic climate effect during the past 2,000 years. However, significant differences between uncertainties associated with different reconstructions have been detected. A previous study used simulations of the past millennium in the Paleoclimate Model Intercomparison Project 3 (PMIP3) and detected an overestimation of global cooling for several years after MVEs and an underestimation of centennial-scale variability in the climate models (Ljungqvist et al., 2019). Moreover, scholars have generated paleo-assimilation data using an assimilation algorithm that combines proxy data and climate simulations (Steiger et al., 2018). Despite the availability of a vast quantity of data, the similarities and differences of the impacts of MVEs on climate reflected by different datasets remain unclear, particularly for China's regional climate and the climate system's main internal variability modes.

In the current research landscape, there is a lack of comprehensive studies that summarize changes in global and Chinese climates, as well as the primary internal climate modes following MVEs during the past 2,000 years. Therefore, we utilized observation, reconstruction, simulation, and assimilation data to address the following questions: (1) What are the methods and data required to accurately reconstruct MVEs over the past two millennia, both globally and specifically in China? (2) What are the temporal and spatial characteristics of temperature and precipitation on interannual-interdecadal time scales following MVEs, and what are the main differences between different datasets? (3) How is the response of the main internal climate modes to MVEs, and what are the associated mechanisms? The insights gained from this study will aid in providing a systematic assessment of the known effects of volcanic forcing affecting past, present, and future climates, which is critical for infrastructure planning, disaster mitigation, food security, and water resource management.

2. Historical facts of volcanic eruptions during the Common Era

2.1 Volcanic forcings and reconstruction methods

The three widely-used volcanic reconstruction datasets during the Common Era (CE) are Gao2008, Crowley2013, and Sigl2015 (Gao et al., 2008; Crowley and Unterman, 2013; Sigl et al., 2015), which are based on reconstructions from ice cores obtained in the vicinity of both the North and South Poles. However, some inconsistencies between the three sets of volcanic forcing data have been detected. For example, from Gao2008, the intensity of the Samalas eruption in 1258 CE is found to be approximately 57% and 31% higher than those from Sigl2015 and Crowley2013, respectively. From 500 to 2000 CE, 132, 301, and 230 volcanic events were detected in Gao2008, Crowley2013, and Sigl2015, respectively.

These differences primarily originate from the original ice core data, reconstruction methods, and judgment criteria (Gao and Gao, 2021). In terms of ice core data, Gao2008 used 36 polar ice core records for reconstruction, with the period of 500–2000 CE. Crowley2013 used 25 polar ice core records for reconstruction, with the period of 800–2000 CE, sharing the same data sources as Gao2008, except for the Taylor dome. Sigl2015 used 22 ice core records from 15 drilling sites where the time coverage of ice core data is relatively uniform, with the period of 500 BCE to 2000 CE. In terms of methodology, Gao2008 identified volcanic signals based on more than twice the 31-year running median absolute deviation, Crowley2013 extracted the signals from each ice core using the point-by-point method, and Sigl2015 identified volcanic signals based on more than three times the 31-year running median absolute deviation. Furthermore, the calculation methods of sulfate deposition in these three datasets were different.

Dating is the fundamental principle of ice core research. Because some large volcanic events (VEI $\geqslant$5) over the past several hundred years, such as the 1991 Pinatubo, 1963 Agung, 1815 Tambora, and 1257 CE Samalas eruptions (Cole-Dai et al., 1997; Lavigne et al., 2013; Sigl et al., 2015), have confirmed occurrence years and geographical locations, they are widely used as volcanic marker horizons in ice core chronologies. Given new materials, technologies, and methods, scholars have recently traced the source of volcanic signals, including the 431 CE Ilopango, 822 CE Katla, and 946 CE Changbaishan eruptions (Büntgen et al., 2017; Oppenheimer et al., 2017; Smith et al., 2020). These additional volcanic markers will further constrain the ice core chronology. However, many "unknown volcanic eruptions" lack clear geographical locations commonly found in the three aforementioned datasets and the Global Volcanism Program (GVP), including the 426 BCE, 536 CE, and 540 CE eruptions, as well as many eruptions with relatively weak intensity (Figure 1). Moreover, the chronology and geographical origins of some sulfur-rich volcanic signals, such as the 1453/1458 CE Kuwae Volcano, remain disputed (Gao et al., 2008; Crowley and Unterman, 2013; Sigl et al., 2015). In the case of volcanic signals without identifiable origins, all three constructions take the same approach, which involves denoting them as tropical eruptions if signals are registered in both poles and mid-to-high latitude eruptions over the corresponding hemisphere. For a tropical eruption, a transfer function value of 1.0×10^9 km^2 is applied in both Gao2008 and Sigl2015 to convert the ice core volcanic deposition over Greenland and Antarctica into stratospheric sulfate aerosol loadings (Gao et al., 2008), which are added together to obtain a global estimate. Similarly, for an extratropical eruption, the transfer function value is set as 0.57×10^9 km^2.

Given the aforementioned volcanic reconstructions, researchers have further extended the time series of volcanic reconstructions in time and space to force general circulation models (GCMs). For example, the volcanic forcing dataset recommended by PMIP4-CMIP6 for the past 1,000/2,000 years includes latitudinally and monthly resolved stratospheric aerosol optical depth, which is obtained by spatiotemporal expansion of the Sigl2015 dataset using the easy volcanic aerosol method (Toohey and Sigl, 2017). The stratospheric transport scheme is calculated by referring to satellite observations of the 1991 Pinatubo eruption.

2.2 Historical facts of volcanic activity

The Gao2008 and Crowley2013 datasets have been applied to the last millennium transient simulations in PMIP3, whereas the Sigl2015 dataset has been recommended for PMIP4 (Jungclaus et al., 2017). During the past 2,000 years, the numbers of tropical, Northern Hemisphere (NH), and Southern Hemisphere (SH) volcanic eruptions were 62, 115, and 56, respectively, and their intensities accounted for 61.7%, 30.5%, and 7.8% of cumulative volcanic forcing in terms of radiative forcing from Sigl2015, respectively (Figure 1). The volcanic reconstructions indicated that intensive MVEs occurred around the periods of 530–700, 1200–1460, and 1600–1840 CE, which were cold epochs, i.e., the Dark Ages Cold Period (DACP, approximately 500–700) and Little Ice Age (LIA, approximately 1250–1800). The quiescent periods occurred during the warm epochs, i.e., the Roman Warm Period (approximately 0–200) and Medieval Climate Anomaly (MCA, approximately 900–1100). For example, the Sigl2015 dataset demonstrates that the average global volcanic intensities are approximately 52.3, 48.5, and 51.9 W m^{-2} (100 yr)$^{-1}$ during the periods of 530–700, 1200–1460, and 1600–1840, respectively, which are remarkably higher than that observed during the quiescent periods of 0–200 and 900–1100, which were 18.7 and 27.0 W m^{-2}(100 yr)$^{-1}$,

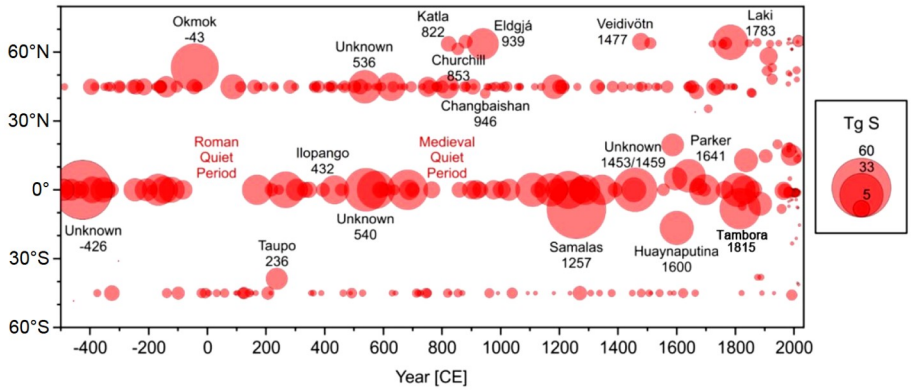

Figure 1 Latitude-time plot of stratospheric volcanic sulfur injections (Tg) from the Sigl2015 dataset during the past 2,500 years. Modified from Figure 6 in Sigl et al. (2022).

respectively. The number of MVEs may contribute to the formation of cold and warm epochs (Miller et al., 2012; Brönnimann et al., 2019); however, the mechanism remains a subject of debate.

According to the volcanic reconstructions, the confirmed volcanic eruptions in China that occurred during the Holocene are shown in Table 1. Six eruptions were observed, each of which exhibited intensities exceeding a VEI of 2. The most recent was the eruption of the Kunlun Volcanic Group on May 27, 1951. The most active volcano in China is the Changbaishan Volcano, which erupted at least seven times during the Holocene. The largest eruption in China was the Changbaishan eruption, which occurred in 946 CE, with a VEI of 6. This eruption is also referred to as the "Millennium Eruption" (Iacovino et al., 2016). The Changbaishan Volcano possesses the greatest disaster potential among all Chinese volcanoes, given that more than 1.6 million people reside within 100 km of its vicinity. Moreover, in the global context, countries surrounding China, such as Japan (83 times), Indonesia (77 times), Russia (57 times), and the Philippines (20 times), have experienced the most frequent volcanic eruptions over the past two millennia (Figure 2).

3. Interannual-interdecadal climate response to MVEs

3.1 Temperature

On the global scale, volcanic eruptions eject sulfate aerosols into the stratosphere, which influence the energy balance of the planet, substantially reducing the global mean surface temperature and affecting large-scale atmospheric circulation (Robock, 2000). For example, observations showed that the global mean surface temperature decreased by 0.5°C one year after the largest volcanic eruption of the past century, the Pinatubo eruption in 1991. All reanalysis datasets showed a similar spatial pattern of surface air temperature (SAT) with a peak cooling of 0.1–0.15°C over latitudes of 60°S–60°N after the 1963, 1982, and 1991 eruptions. However, divergent responses occurred in the polar regions (Fujiwara et al., 2020).

To investigate the temporal change of global SAT after MVEs, we used reconstructions and simulations. The global mean temperature reconstructions were derived using seven different statistical methods (Neukom et al., 2019). Climate simulations included transient experiments in the past millennium using the BCC-CSM1-1, CCSM4, CSIRO-Mk3L-1-2, FGOALS-s2, GISS-E2-R, HadCM3, IPSL-CM5A-LR, MPI-ESM-P, MRI-CGCM3, MIROC-ES2L, and MRI-ESM2-0 from the PMIP3/4 as well as the ensemble mean of all-forcing experiments from the Community Earth System Model-Last Millennium Ensemble (CESM-LME) (Jungclaus et al., 2017; Otto-Bliesner et al., 2016). Reconstructions showed that extreme global cooling events occurred after the 11 largest MVEs, particularly for years such as 1601, 1641, 1699, 1815, and 1457 CE. These rank among the top 30 coldest years from 850 to 2000 (Figure 3b). Some proxies also indicated that a particularly cold summer occurred in Europe and the Arctic one year after the 1815 Tambora eruption, often referred to as the "year without a summer", leading to widespread famine and agricultural failure in Europe (Luterbacher and Pfister, 2015). Climate simulations reproduced the extreme cold events of 1601, 1641, 1699, 1815, and 1457 CE, which are attributable to volcanic eruptions (Figure 3c). However, while simulations identified 1259 as the coldest year following the Samalas eruption, reconstructions only revealed moderate cooling.

Over China, many studies have discussed the temperature changes after volcanic eruptions. We used observation, reconstruction, simulation, and assimilation data to comprehensively understand spatiotemporal changes in SAT over China after MVEs. We used reconstruction data from Ge2013, Shi2012, Cook2013, Shi2015, and Zhang2018 (Ge et al., 2013; Shi et al., 2012; Cook et al., 2013; Shi et al., 2015; Zhang et al., 2018). Ge2013 and Shi2012 are the annual mean temperature reconstructions over China.

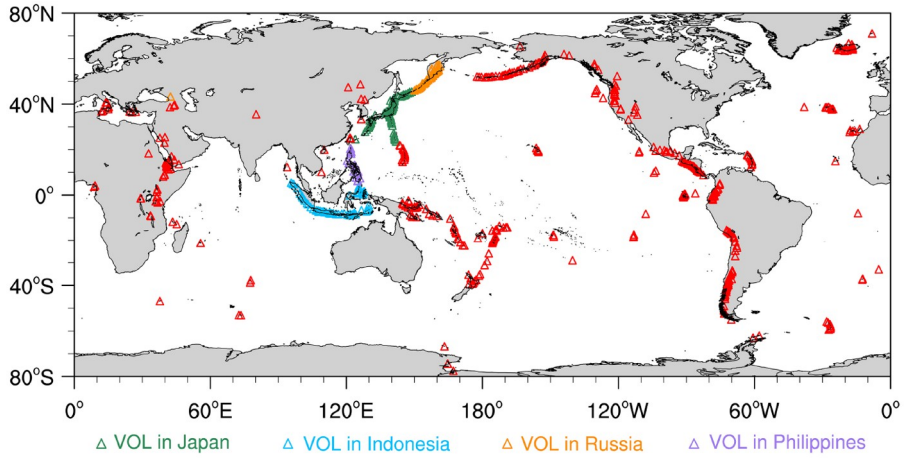

Figure 2 Distribution of volcanic events during the past two millennia according to the Global Volcanism Program dataset. The green, blue, orange, and purple triangles represent the volcanic eruptions over Japan, Indonesia, Russia, and the Philippines, respectively, whereas the red triangles denote other eruptions.

Table 1 Confirmed Holocene eruptions from volcanoes in China according to the Global Volcanism Program (GVP) dataset

Volcano name	Location	Population within 100 km	Known eruption year	VEI	References
Arxan–Chaihe	47.45° N 120.8° E	>0.1 million	0 ± 150		GVP
Changbaishan	41.98° N 128.08° E	>1.6 million	2160 BCE ± 100 180 BCE ± 75 946 Nov 1668 Jun 1702 Jun 1898 1903 Apr	4 4 6 2	Wei et al., 2013; Iacovino et al., 2016; Oppenheimer et al., 2017
Hainan Volcanic Field	19.905° N 110.229° E	>6.2 million	1883 1933 Jun		GVP
Jingpohu	44.08° N 128.83° E	>2.3 million	3550 BCE 1540 BCE ± 150 520 BCE ± 100		GVP
Kunlun Volcanic Group	35.52° N 80.2° E	>22 thousand	1951 May 27	2	GVP
Longgang Group	42.33° N 126.5° E	>4.4 million	350		GVP
Tengchong Group	25.23° N 98.5° E	>2.9 million	5750 BCE ± 1000		GVP
Wudalianchi	48.722° N 126.15° E	>2.1 million	1721 Jun	3	Wei et al., 2013

Cook2013 and Shi2015 are the Jun–Aug (JJA) mean temperature reconstructions over East Asia and Asia, respectively, while Zhang2018 denotes the warm season (May–Sep) East Asian temperature. Assimilation data included the Paleo Hydrodynamics Data Assimilation product (PHYDA) (Steiger et al., 2018).

First, we analyzed temporal variation in average SAT across East Asia on the interannual time scale. We used Cook2013 and PHYDA data due to their annual resolution (Figure 4b). Cook2013 data showed that over the past 1,200 years, the 11 largest MVEs caused six extremely cold summers, ranking among the top 50 coldest events in history. In particular, eruptions in years such as 1234, 1819, and 1459 CE ranked as the first, fourth, and sixth coldest events, respectively, which is similar to previous work on NH temperature reconstructions (Schneider et al., 2017). PHYDA data also showed a similar temperature response to MVEs after 1600 CE. However, the 946 CE Changbaishan and 1721 CE Wudalianchi eruptions, which occurred in China, had no significant impact on the temperature in China (Figure 4b). A

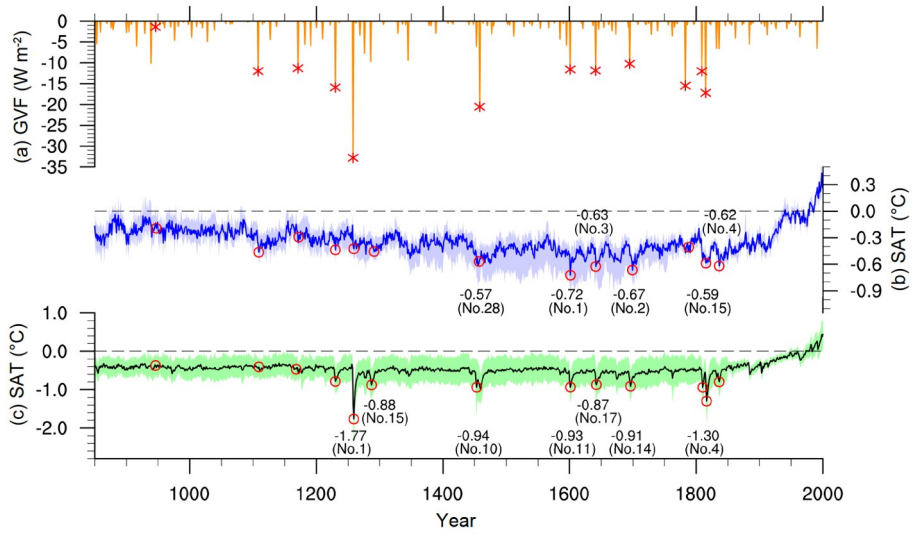

Figure 3 Time series of global surface air temperature (SAT) over the past millennium. (a) Reconstruction of global volcanic forcing (GVF, W m^{-2}) (Sigl et al., 2015). The asterisks mark the 11 largest MVEs and the 946 CE Changbaishan eruption. (b) Reconstructed surface temperature anomalies (°C) relative to 1961–1990 (Neukom et al., 2019). The shading indicates the range of seven reconstruction methods. The red circles denote the minimum values of temperature anomalies within four years after the 11 largest MVEs and the 946 CE Changbaishan eruption. (c) Ensemble mean of annual mean SAT anomalies (°C) from multi-model simulations (black line). The shading indicates the one standard deviation interval.

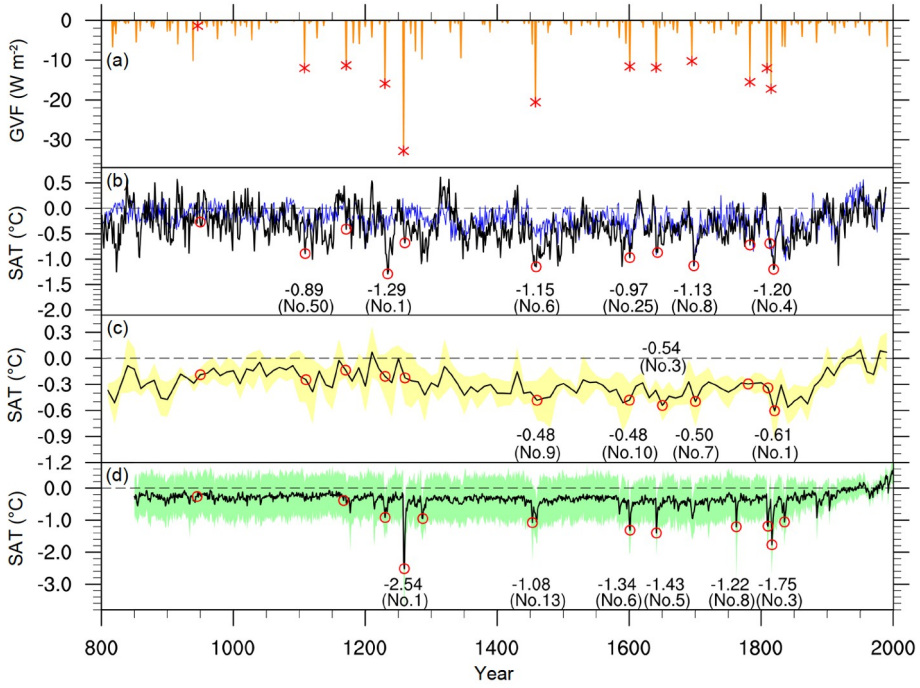

Figure 4 Time series of East Asian surface air temperature (SAT) over the past millennium. (a) Reconstruction of global volcanic forcing (GVF, W m^{-2}) (Sigl et al., 2015). The asterisks mark the 11 largest MVEs and the 946 CE Changbaishan eruption. (b) Reconstructed June to August (JJA) mean surface temperature anomalies for East Asia (°C), relative to 1961–1990. The black line denotes the reconstruction of Cook2013, whereas the blue line denotes the assimilation of the Paleo Hydrodynamics Data Assimilation product (PHYDA). The red circles denote the minimum values of temperature anomalies within four years after the 11 largest MVEs and the 946 CE Changbaishan eruption. (c) Ensemble mean of five temperature reconstructions (°C) from Ge2013, Shi2012, Cook2013, Shi2015, and Zhang2018. The yellow shading denotes the one standard deviation interval. (d) Ensemble mean of JJA mean temperature anomalies (°C) over East Asia (20°–55°N, 70°–140°E) from 12 PMIP models. The green shading denotes the one standard deviation interval.

muted climatic response to the Changbaishan eruption was also observed in NH or global temperature reconstructions (Oppenheimer et al., 2017) (Figure 3b), and Greenland ice cores only recorded a weak sulfate signal (Iacovino et al., 2016). This may be related to the latitude and season of the eruption. Stratospheric volcanic aerosols can be shorter-lived following an eruption in mid-to-high latitudes (i.e., Changbaishan) compared to an eruption in the tropics. The

Changbaishan eruption might erupt during the NH winter of 946 CE (Oppenheimer et al., 2017), when the removal of stratospheric volcanic aerosols was enhanced in the Arctic region. This could be attributed to strong subsidence in the polar vortex during winter (Gao et al., 2008) and a higher burden and residence time of SO_2, causing less efficient oxidation of SO_2 to H_2SO_4, compared to a summertime eruption (Schmidt et al., 2010).

To determine spatial variations in temperature after MVEs, we used SAT data from the Climatic Research Unit (CRU) (Brohan et al., 2006), Cook2013, climate simulations, and PHYDA. During the period with instrumental data, large volcanic eruptions occurred in 1963, 1982, and 1991. In the first winter after these eruptions, superposed epoch analysis showed that most parts of China experienced significant cooling, with a range lower than −1°C (Figure 5a). The multi-model ensemble results showed a significant decrease in temperature only over northern China (Figure 5b). PHYDA data showed that temperature decreased significantly over eastern and northwestern China, while anomalous warming occurred over the Tibetan Plateau (Figure 5c). In the first summer, CRU instrumental data indicated strong cooling in central and northeastern China (Figure 5d); however, modeling data indicated insignificant cooling over China and PHYDA data showed moderate cooling between observations and simulations (Figures 5d–5f). In the first summer after the ten largest tropical MVEs between 850 and 1850 CE, Cook 2013 data showed significant cooling in most parts of China except for the Yangtze River Basin and southern China (Figure 5g). However, simulation data showed consistent cooling across China, particularly on the Tibetan Plateau (Ning et al., 2019), with a greater cooling amplitude than that in reconstruction data (Figure 5h). PHYDA data indicated a similar cooling amplitude to Cook2013 data but with a cooling center in eastern China (Figure 5i).

It should be noted that the intensities of the ten largest tropical MVEs during 850–1850 CE were approximately 4.4 times greater than those of the three volcanic eruptions during the instrumental period, but Cook2013 and PHYDA data indicated that the amplitude of anomalous cooling in China after the ten largest tropical MVEs was nearly identical to that after the three observed volcanic eruptions (Figure 5d, 5f, 5g, 5i). Meanwhile, after the largest eruption of the past 2000 years (i.e., the 1257 CE Samalas eruption), no significant cooling was indicated in Cook2013 or PHYDA data (Figure 4b). For climate simulations, volcano-induced cooling in China exhibited a significant linear relationship with volcanic intensity (Figures 4d and 5b, 5e, 5h), which was overestimated compared with that in reconstructions. However, after three observed volcanic eruptions, the simulated cooling in winter and summer in China was significantly underestimated compared with instrumental data (Figures 5a–5f).

We inferred that inconsistencies between observed, reconstructed, and simulated temperature responses to MVEs may have the following explanations: (1) MVEs do not cause globally or regionally uniform cooling, and internal variability may affect the signal and magnitude of temperature anomalies (Cook et al., 2013). For the regional temperature response to volcanic forcing on the interannual time scale, two major delayed climate factors are the El Niño-Southern Oscillation (ENSO) and the North Atlantic Oscillation (NAO) (Xing et al., 2020). These two modes can significantly modulate temperature in China through atmospheric teleconnection, particularly boreal winter temperature. Comparison between reconstructions with large sample sizes and three observed volcanic eruptions should be done carefully because interannual variability may dominate for the latter. Numerical models also encounter problems in simulating these delayed responses (Xing et al., 2020). (2) There may be some uncertainty in the reconstructed data, such as reduced sensitivity to cooling in trees that grow near the tree line (Mann et al., 2012). (3) There is also a large uncertainty associated with estimated volcanic forcing (Toohey and Sigl, 2017), climate model stratospheric chemistry, and microphysical processes (Stoffel et al., 2015; Zanchettin et al., 2016). (4) The climate background during 850–1850 CE was different from that in the modern warm period, and volcano-induced cooling effects may be stronger in a warmer climate (Fasullo et al., 2017).

To detect volcanic impacts on the interdecadal variation of temperature in China, we used the ensemble mean of five temperature reconstructions from Ge2013, Shi2012, Cook2013, Shi2015, and Zhang2018 (Figure 4c). We determined that MVEs induced significant cooling at 1815–1825, 1645–1655, 1695–1705, and 1455–1465 CE, which ranked as the first, third, seventh, and ninth coldest decades over the past 1,200 years, respectively. MVEs frequently occurred during these four cold decades. Using NH multiproxy records, previous studies have also observed similar trends where the coldest decades follow clusters of MVEs, particularly for the middle of the fifteenth and seventeenth centuries and early nineteenth century (Sigl et al., 2015); this finding is also reflected in modeling results (Figure 4d).

Overall, data showed significant cooling throughout the globe and China several years after MVEs and interdecadal-scale cold events in NH and China when major and successive moderate volcanoes erupted. However, there is a large spread of magnitude of cooling between different data. Reconstructions. The reconstructions and assimilations showed that the magnitude of cooling is not completely consistent with the intensity of MVEs, but the magnitude of cooling simulated by PMIP models has a significant linear relationship with volcanic intensity, which is overestimated compared with that in reconstructions. This model-data

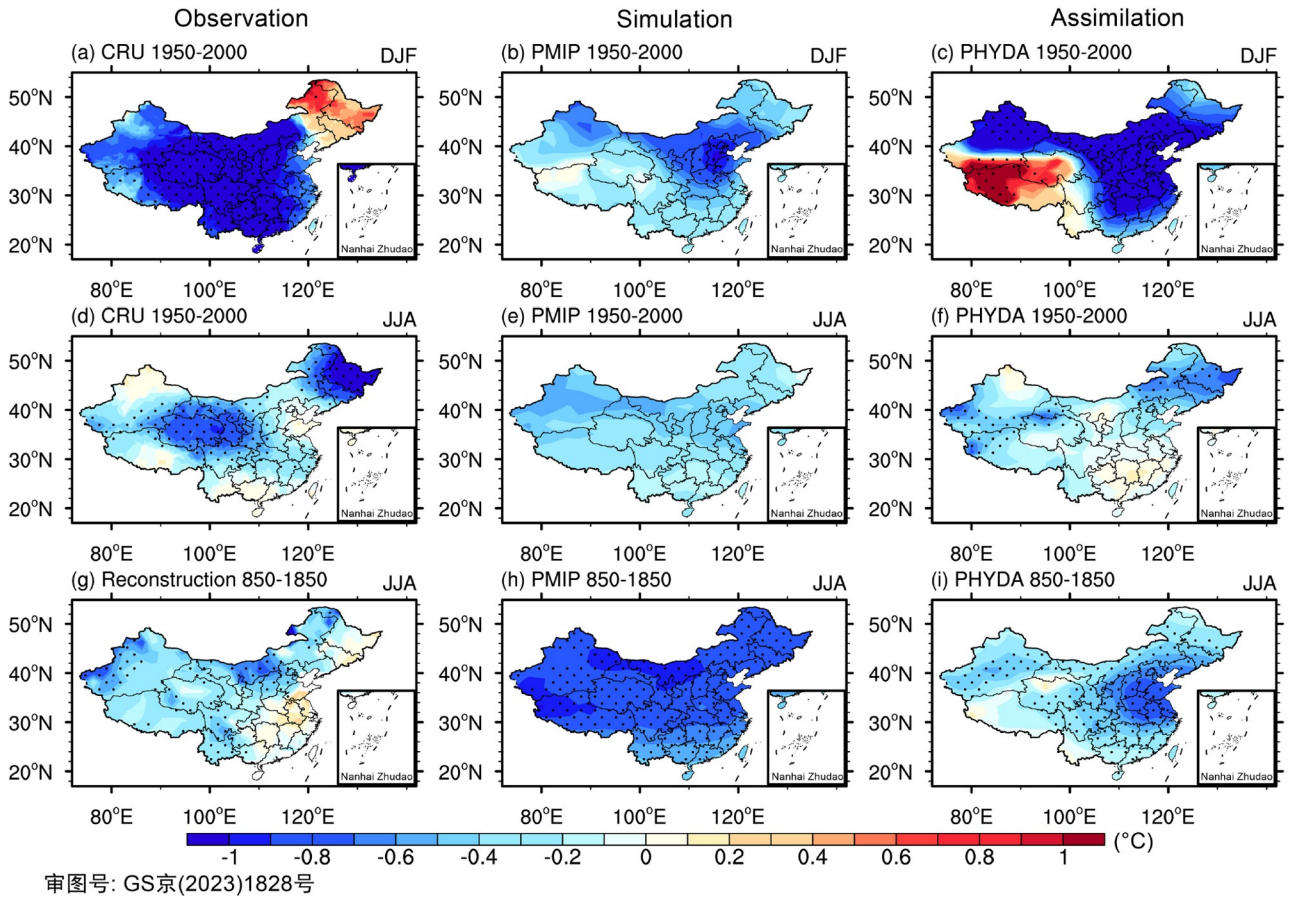

Figure 5 SAT response after tropical MVEs. ((a)–(c)) Superposed epoch analysis (SEA) of temperature anomalies in the first winter after the 1963, 1982, and 1991 eruptions based on datasets of the Climatic Research Unit, 12 PMIP models, and PHYDA. ((d)–(f)) Same as ((a)–(c)), but for the first summer. ((g)–(i)) SEA of temperature anomalies in the first summer after the ten largest tropical MVEs during the period of 850–1850 CE, based on datasets of Cook2013, 12 PMIP models, and PHYDA. The SCS represents the South China Sea. The anomalies are calculated by removing the mean of the five years before the eruption. The dotted areas exceed 95% confidence levels based on bootstrap resampling (n=10,000).

disagreement could be caused by internal variability and uncertainties in the reconstructed methods and aerosol–climate model and climate background.

3.2 Precipitation

On a global scale, a decrease in global and monsoonal precipitation after MVEs was observed (Iles et al., 2013; Liu et al., 2016). Specifically, using instrumental data and CMIP5 historical runs, several scholars determined that global precipitation, atmospheric humidity, and monsoonal precipitation were reduced after four large volcanic eruptions from the 1960s onward (Paik and Min, 2017). Based on reconstructions and simulations over the past millennium, volcanic eruptions tend to decrease monsoonal precipitation in the hemisphere in which they occur while enhancing monsoonal precipitation in the opposing hemisphere (Liu et al., 2016; Zuo et al., 2019). Tropical volcanic eruptions reduce tropical monsoonal precipitation mainly by reducing atmospheric humidity and land-sea thermal contrast. However, modeling results usually underestimate global precipitation reduction (Tejedor et al., 2021) and have uncertainties in the spatial distribution of precipitation after MVEs, which may be related to divergent ENSO responses, the pre-eruption climate background, and the season of eruption. (Stevenson et al., 2017; Sun et al., 2019b; Paik et al., 2020).

The mechanism of the change in precipitation in China after tropical MVEs is controversial. A popular view is that tropical MVEs weaken the East Asian summer monsoon (EASM) and precipitation in eastern China, inducing droughts (Peng et al., 2010; Man et al., 2014; Chen et al., 2020). This conclusion is mainly based on model simulations and reconstructed dry-wet indices in eastern China (Zheng et al., 2006). The Tree-ring-based Palmer Drought Severity Index reconstructions also showed that after the 1815 CE eruption, a drought occurred across most of China, whereas a wet condition occurred over the Yangtze River Basin (Gao et al., 2017). Furthermore, the assimilation data indicated that substantial droughts have occurred in north and northwest China in 1–4 years after tropical volcanic eruptions during the past millennium (Tejedor et al., 2021). Previous studies

showed that volcano-induced cooling led to a weakened summer land-sea thermal contrast, which in turn weakened the EASM. Simultaneously, a reduced atmospheric moisture content and soil moisture feedback further reduced the EASM precipitation (Chen et al., 2022b).

An alternative explanation is that the EASM precipitation is enhanced after tropical MVEs, modulated by a volcano-induced El Niño (Liu et al., 2022a). Using three well-known precipitation reconstructions (Feng et al., 2013; Shi et al., 2017, 2018), Liu et al. (2022a) found a marked increase in precipitation over the Yangtze River Basin and northeast China, accompanied by decreased precipitation over the Philippines and Indo-China Peninsula after 22 tropical volcanic eruptions during the period of 1470–1999 CE. This pattern resembles the observed precipitation anomaly pattern in summer following the mature stage of El Niño (Zhang et al., 1996; Wang et al., 2000). Several scholars also observed a meridional dipole pattern with a wetter Yangtze–Huaihe river valley and drier southern China after 13 large tropical eruptions over the past 500 years (Gao and Gao, 2018).

To comprehensively understand the response of precipitation in China to tropical MVEs, we examined the observed precipitation from the Global Precipitation Climatology Centre (GPCC) (Schneider et al., 2014), reconstructed precipitation from the Shi2018 reconstruction, PMIP multi-model simulations, and PHYDA over the past five centuries. In the first summer after three observed eruptions (i.e., 1963, 1982, and 1991), precipitation increased in south and northeast China but decreased to the north of the Great Khingan Mountains and in the south and southeast Asia (Figure 6a). By contrast, the climate models reveal a weak dry condition over south China, the southern Tibetan Plateau, and south Asia (Figure 6b), whereas PHYDA shows a strong wet center over northwestern China (Figure 6c).

In the first summer after the five largest tropical MVEs in the period of 1470–1850 CE, the reconstructions show wet conditions over the Yangtze River Basin, northeast China, and the southern Tibetan Plateau (Figure 6d), which is similar to an enhanced EASM precipitation pattern. The modeling data indicate a decrease in precipitation over northern China and the southern Tibetan Plateau and an increase over the Yangtze River Basin (Figure 6e). The precipitation anomaly pattern in PHYDA is similar to the modeling results but with stronger magnitude (Figure 6f). Thus, although the reconstruction, simulation, and assimilation data indicate an increase in precipitation over the Yangtze River Basin after tropical MVEs, they reveal a divergent response over other regions, such as north and northeast China and the southern Tibetan Plateau.

Volcanic eruptions can also contribute to decadal droughts. First, successive volcanic eruptions may induce decadal droughts. Observations showed that Asian summer monsoon precipitation was considerably weaker during the periods of 1901–1935 and 1963–1993, when volcanic activity was more frequent, compared with that during the inactive vol-

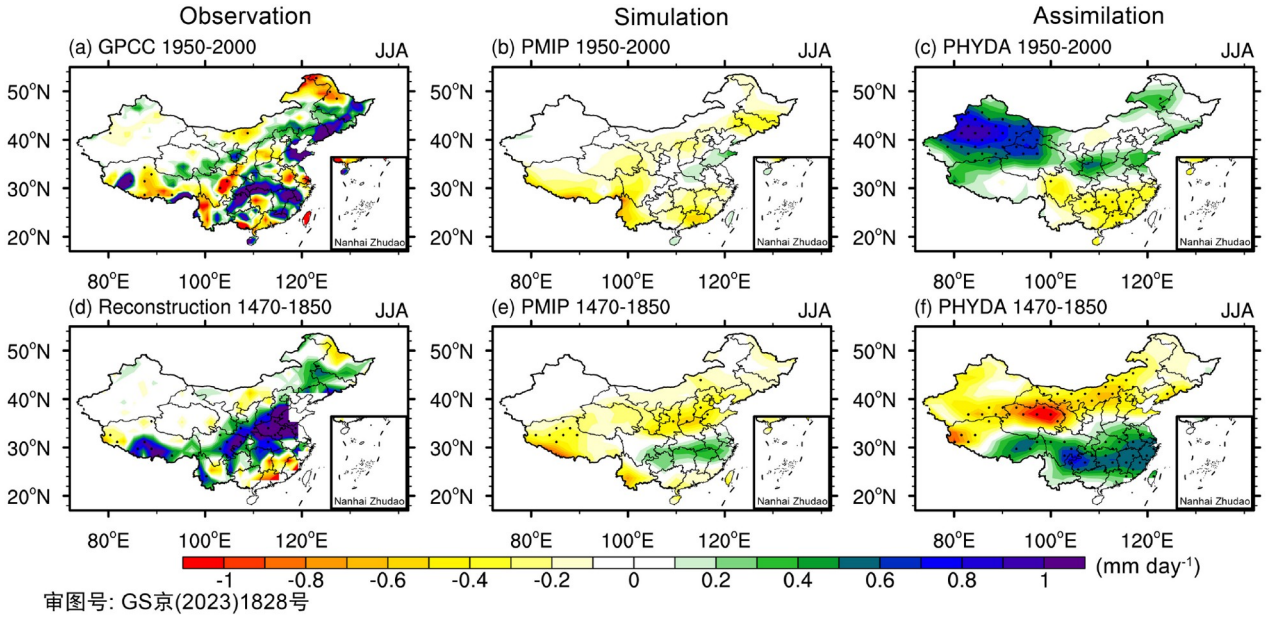

Figure 6 Precipitation response after tropical MVEs. ((a)–(c)) SEA of precipitation anomalies in the first summer after the 1963, 1982, and 1991 eruptions, based on datasets of the Global Precipitation Climatology Center, 12 PMIP models, and PHYDA. ((d)–(f)) SEA of precipitation anomalies in the first summer after the five largest tropical MVEs during the period of 1470–1850 CE, based on the datasets of Shi2018, 12 PMIP models, and PHYDA. The SCS represents the South China Sea. The anomalies are calculated by removing the mean of five years before the eruption. The dotted areas exceed 95% confidence levels based on bootstrap resampling (n=10,000). In PHYDA, the results correspond to the standardized precipitation evapotranspiration index (SPEI).

canic period of 1936–1962 (Ning et al., 2017). Proxy data showed that under the 536, 540, and 547 CE eruptions, the NH experienced substantial decadal cooling and drought, which is considered one of the triggers for the DACP (Büntgen et al., 2016). Similarly, at the end of the LIA (approximately 1800s–1840s), a sequence of large eruptions continuously weakened the global monsoon (Brönnimann et al., 2019). Second, the combination of volcanism and other external forcings can also cause decadal droughts. Using the reconstructed dry-wet index of northern China (Zheng et al., 2006), scholars selected five periods of strongest decadal megadroughts (i.e., 1146–1155, 1240–1249, 1483–1492, 1578–1587, and 1634–1643 CE) and found similar decadal dry conditions over North America and Europe (Bai et al., 2019). Nine PMIP3 past millennium simulations also show this phenomenon, caused by both strong volcanic eruptions and weak solar irradiation. Furthermore, the superimposition of internal variability and volcanism can aggravate decadal droughts (Ning et al., 2020). The late Ming Dynasty megadrought (1637–1643) was probably triggered by internal variability; meanwhile, the 1641 Parker eruption extended the drought (Chen et al., 2020; 2022b). Thus, continuous volcanic eruptions, the combined effect of volcanism and low solar irradiation, and internal variability superimposed on volcanism may cause decadal droughts, which may, in turn, contribute to famine, wars, and social unrest (Büntgen et al., 2016; Hao et al., 2020; Gao et al., 2021).

In general, in the first summer after tropical MVEs, a decrease in global and monsoonal precipitation and an increase in precipitation over the Yangtze River Basin occurred. Frequent volcanic eruptions, volcanism superimposed on low solar irradiation, and internal variability superimposed on volcanism may cause decadal droughts over NH monsoon regions and eastern China. Divergent responses are found over north and northeast China and the southern Tibetan Plateau using different data, indicating that the impact of MVEs on regional precipitation (i.e., China) is complex. In particular, large uncertainty is a likely consequence of diverse internal climate modes' response and feedback to MVEs.

4. Main internal climate modes response to MVEs

4.1 El Niño–Southern Oscillation

The ENSO is one of the most important sources of internal variability in the climate system on the interannual time scale. During the twentieth century, instrumental data showed that although El Niño occurred after the 1982 El Chichón and the 1991 Pinatubo eruptions, these eruptions occurred during the ongoing development of El Niño, indicating a more coincidental relationship (McGregor and Timmermann, 2011). Because of a lack of tropical MVEs during the instrumental period, the response of ENSO to volcanic eruptions remains a subject of debate.

One view is that an El Niño event occurs after a large tropical volcanic eruption. This view has been put forward on the basis of tree rings and other reconstructed data from the past millennium (Adams et al., 2003; Li et al., 2013). Climate models also showed that tropical MVEs considerably increase the probability of an El Niño event (Emile-Geay et al., 2008; Liu et al., 2018a), and the following potential triggering mechanisms have been proposed: (1) Tropical MVEs cause the tropical land mass to be colder than equatorial Pacific SST, leading to a land-sea thermal contrast over Maritime Continent and anomalous equatorial westerlies (Ohba et al., 2013). (2) Tropical MVEs induce a zonal SST gradient over the equatorial Pacific through the ocean thermostat (Clement et al., 1996). (3) Tropical MVEs enhance the equatorial westerly anomalies in the western Pacific by causing land cooling, which weakens the monsoon (e.g., North African monsoon) and excites the atmospheric Kelvin wave (Khodri et al., 2017; Liu et al., 2022b). Most models can simulate monsoon suppression-induced equatorial westerly wind anomalies (Chai et al., 2020), which could result in the development of El Niño (Chen et al., 2015).

Supported by this view of volcano-induced El Niño events, some scholars have determined that tropical MVEs affect the global climate through El Niño-related atmospheric teleconnection. The decay of a tropical MVE-induced El Niño event can be stronger than that of a nonvolcanic El Niño event (Sun et al., 2019a), inducing an anomalous western North Pacific anticyclone (WNPAC) (Zhang et al., 1996; Wang et al., 2000), which transports moisture to the Yangtze River Basin via anomalous southwesterly winds (Liu et al., 2022a). In the second year following a tropical MVE, a significant La Niña-like state has been shown to occur (Sun et al., 2019a), contributing to the enhancement of the East Asian winter monsoon and cooling over China. Meanwhile, under tropical MVEs, the enhanced ENSO frequency can further strengthen the coupling of ENSO and the Indian monsoon during years +1 to +4 (Singh et al., 2020). The PHYDA data also reveal significant dry conditions over Central Asia and tropical Africa after tropical MVEs, which persist for >4 years (Tejedor et al., 2021). However, GCMs produce a weak and less persistent regional response, the origins of which can be traced to divergent ENSO responses, structural components of models, and inaccurate estimates of volcanic forcing across different simulations (Tejedor et al., 2021).

An alternative view is that no clear El Niño event occurred after tropical MVEs. On the basis of the long and high-resolution coral $\delta^{18}O$ records from Palmyra Island over the central tropical Pacific, Dee et al. (2020) observed an in-

significant El-Niño-like response to tropical MVEs over the past millennium. In particular, the $\delta^{18}O$ values of Palmyra corals were insensitive to the 1257 CE Samalas mega eruption. Furthermore, Zhu et al. (2022) used the data assimilation algorithm of the Last Millennium Reanalysis (LMR) to assimilate coral records (Dee et al., 2020) and tree rings (Li et al., 2013), both separately and together, which revealed only a weak relationship between El Niño and tropical MVEs. These studies showed that the strong tropical MVE-ENSO relationship revealed by tree-ring records is not robust because midlatitude tree-ring data are mixed with ENSO-teleconnection signals and local changes in temperature and precipitation. Moreover, some GCMs show no significant warming over the equatorial eastern Pacific after tropical MVEs, supporting the view of a weak tropical MVE-ENSO relationship (McGregor and Timmermann, 2011). However, this view has been called into question. Robock (2020) proposed that the coral records in the tropical central Pacific only reflect the actual local SST and not the SST change relative to the rest of the tropics (i.e., relative SST) because the entire tropical SST decreases following tropical MVEs, which can offset the El Niño warming.

Thus, based on the tree-ring and climate modeling data, tropical MVEs can induce an El Niño event over the past millennium. Subsequently, El Niño decays rapidly, which causes WNPAC and increases the summer precipitation over the Yangtze River Basin. Alternatively, the coral $\delta^{18}O$ records over the central tropical Pacific indicate no significant El Niño response to tropical MVEs.

4.2 Atlantic Multidecadal Oscillation

The Atlantic Multidecadal Oscillation (AMO) considerably impacts interdecadal changes in both global and Chinese climates (Zhang et al., 2019). Instrumental data revealed the existence of a negative phase of AMO during the active volcanic periods of 1901–1935 and 1963–1993, while a positive phase of AMO existed during the inactive volcanic period of 1936–1962, which in turn affected the Asian and global monsoon (Ning et al., 2017). With the climate model simulations, previous studies proposed that volcanic and anthropogenic aerosols are the primary reasons for the AMO phase (Otterå et al., 2010; Booth et al., 2019). However, this contradicts the conventional view that the AMO is controlled by internal variability (Clement et al., 2015; Zhang et al., 2019). Currently, the relative contributions of external forcing and internal variability to the AMO remain controversial.

In order to gain a deeper understanding of the influence of external forcing (volcanic eruption) on the AMO, we focused on the period spanning the past two millennia, during which human activities had minimal effects. Some reconstructed AMO indices indicate negative AMO anomalies during the decade following MVEs (Wang et al., 2017). Using the reconstruction, assimilation, and simulation data, scholars found that when the total sulfate aerosol loading of a tropical volcanic eruption was >30 Tg, a significant negative AMO phase occurred, regardless of the initial conditions before the eruption (Chen et al., 2022a). In particular, during the LIA, the reconstruction data showed an evident quasi-60-year cycle in the AMO (Mann et al., 2009; Lapointe et al., 2020) (Figure 7). Meanwhile, the intensity of volcanic activity was strong and frequent, with a 50–70-year cycle. By comparing the assimilation data with the PMIP3/4 all-forcing, control, and volcanic forcing experiments, the internal mode of the AMO is determined to be a 40-year cycle, and volcanic activity forcing could extend the AMO periodicity to 50–70 years (Mann et al., 2021; Dai et al., 2022) (Figure 7). However, the common AMO definition (i.e., SST over the North Atlantic) may include the global cooling background affected by volcanism, rather than the variability of the AMO. After removing the global cooling background, the impact of volcanism on the AMO is significantly weakened (Michel et al., 2022). This method may also excessively eliminate the contribution of external forcing, which remains controversial.

Changes in the phase, intensity, and periodicity of the AMO under the influence of MVEs may further affect the climate. Some simulation data have revealed that the relationship between the North Pacific Ocean and the North Atlantic Ocean is closer after MVEs (Zanchettin et al., 2012). The comparison of the reconstruction, assimilation, and simulation data showed that the 50–70-year AMO variability may affect the Pacific Ocean through atmospheric processes, resulting in multi-decadal (i.e., 50–70 years) Pacific Decadal Oscillation (PDO)-like variability during the LIA (Sun et al., 2022). At the end of the LIA (i.e., the first half of the 19th century), frequent large volcanic eruptions may have caused a negative AMO phase (Knudsen et al., 2014), further weakening the Afro-Asian summer monsoon and decreasing the East Asian temperature (Brönnimann et al., 2019). It should be noted that there is also a possibility that volcanic forcing induces a “resonant” behavior between the weakened monsoon and the negative AMO phase rather than affecting the monsoon through the AMO (Stevenson et al., 2018; Shen et al., 2022). However, the direct volcanic effect on climate from the indirect effect caused by the modulation of the AMO is still difficult to distinguish.

Several potential mechanisms by which volcanic forcing can affect the AMO have been proposed; these include the following:

(1) MVEs can affect the North Atlantic through sea ice processes. Large MVEs cause a decadal-scale or centennial-scale enhancement of the extent of Arctic sea ice, consequently resulting in sea-ice-albedo feedback, reducing the summer surface net shortwave radiation (Schneider et al.,

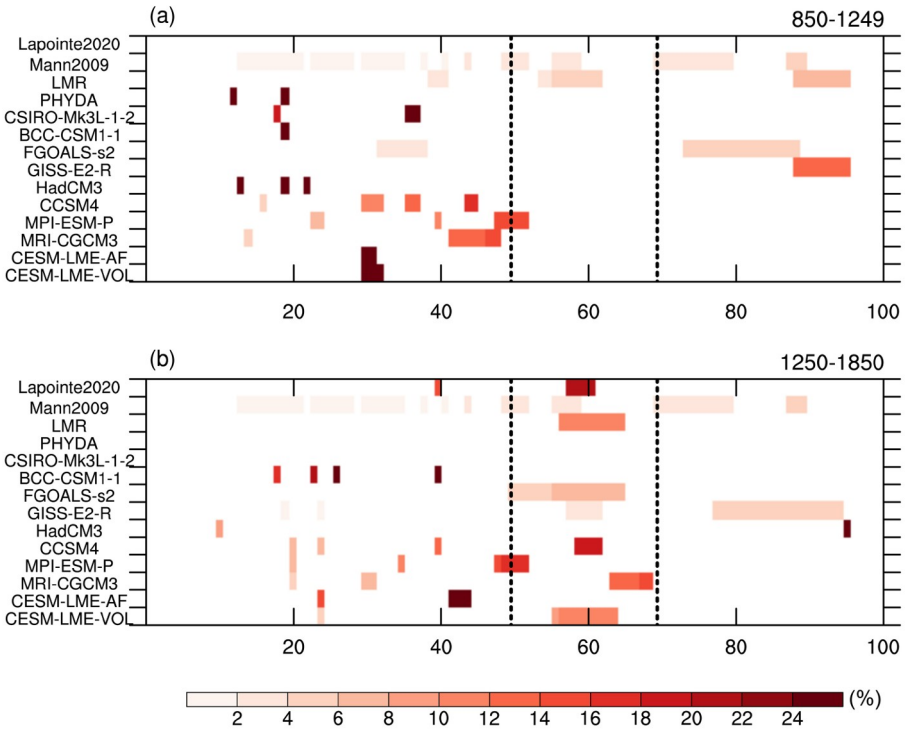

Figure 7 Power spectrum analysis of the AMO derived from reconstructed, assimilated, and simulated data during the periods of 850–1249 CE (a) and 1250–1850 CE (b). Lapointe2020 and Mann2009 are the AMO reconstructions (Lapointe et al., 2020; Mann et al., 2009), whereas Last Millennium Reanalysis (LMR) and PHYDA are the assimilations (Tardif et al., 2019; Steiger et al., 2018). The black vertical dashed lines denote the 50–70-yr periodicities. Only the significant power values with confidence levels exceeding 90% are shaded.

2009; Liu et al., 2018b; Sun et al., 2021; Chen et al., 2022b). Volcano-induced sea ice expansion also reduces the surface longwave radiation from the ocean to the atmosphere in winter, strengthening local cooling (Liu et al., 2020). Meanwhile, sea ice expansion reduces the convection intensity over the subpolar North Atlantic, freshening the surface seawater and weakening the subpolar gyre, consequently reducing the transport of heat and salinity to the Arctic Ocean and decreasing the rate of basal ice melt, thereby maintaining sea ice (Zhong et al., 2010). Subsequently, the melting of expanded sea ice injects freshwater into southern Greenland, decreasing sea surface salinity, suppressing ocean convection, and reducing northward warm water transport (Dai et al., 2022).

(2) MVEs may affect the AMO by modulating the NAO. A positive NAO phase was formed two years after tropical MVEs, according to the observed 1991 Pinatubo eruption and reconstructed NAO index from the past millennium (Ortega et al., 2015). This finding can be related to the change in polar temperature gradient caused by aerosols heating the stratosphere, which enhances the covariability of NAO-related winds and SST over the North Atlantic (Zanchettin et al., 2012). Specifically, the positive NAO phase strengthens the midlatitude westerlies over the North Atlantic, which enhances evaporation and latent heat release, transports cold water eastward, and decreases the subpolar SST, thereby improving the subtropical high and anticyclonic circulation and strengthening the easterly wind over the tropical North Atlantic, consequently increasing the local evaporation, shallowing the thermocline, and further reducing the tropical North Atlantic SST. Consequently, a "horseshoe" cooling pattern is formed over the North Atlantic.

(3) Long-term changes in the Atlantic meridional overturning circulation (AMOC) after MVEs may further affect the AMO. Many GCMs have simulated a decadal-scale enhancement of AMOC after MVEs, followed by a few decades of reduction in the AMOC (Zanchettin et al., 2012; Slawinska and Robock, 2018). During the AMOC development period, the MVE-induced positive NAO extracts heat from the Labrador Sea and subpolar gyre, increasing sea surface salinity and oceanic convection and strengthening the AMOC as a result. MVEs also suppress the global water cycle and shift the storm track southward, which decreases the Arctic precipitation and the associated river runoff, thereby increasing the near-surface density of the Greenland Sea and causing an enhanced AMOC and northward heat transport (Iwi et al., 2012). However, the subpolar sea-ice cover reduces the surface water temperature and salinity, and Arctic sea ice reduces ice production and brine rejection in the Arctic Ocean, decreasing the oceanic convection, which contributes to AMOC weakening (Zhong et al., 2010). When

subpolar sea ice melts, it injects freshwater into the ocean and decreases sea surface salinity (Dai et al., 2022); consequently, northward heat transport in the ocean is reduced. However, some modeling studies have found that no remarkable enhancement occurred; rather, a sustained reduction in northward heat transport in the North Atlantic occurred after MVEs (Miller et al., 2012). This finding indicates that there is currently no robust understanding of the volcanic impact on the AMOC; this might be related to model uncertainty in simulating the AMOC dynamics and the effects of different initial conditions.

Overall, most studies showed that frequent MVEs contribute to a cold AMO phase and extend the periodicity of the AMO but the mechanism remains unclear. Several potential mechanisms have been proposed: Volcanic forcing affects the AMO by modulating the sea-ice processes, the positive phase of NAO, and the long-term changes in the AMOC. However, the common AMO definition (i.e., SST over the North Atlantic) may include the global cooling background affected by volcanism rather than the variability of the AMO. In the future, more research should be conducted to effectively extract the AMO mode and its response to volcanic forcing.

5. Directions for future research

5.1 Volcanic aerosol evolution and its impact on climate under different climate backgrounds

Previous studies focused on the initial conditions before a volcanic eruption, particularly the internal variability (e.g., ENSO and AMO). Under global warming, the climate background changes considerably and rapidly. Notably, the increase in troposphere height in the future warming scenario will reduce the amount of stratospheric sulfate aerosols after moderate volcanic eruptions (VEI of 3–5) and reduce radiative forcing (Aubry et al., 2021). However, the impact of large volcanic eruptions will be markedly enhanced through increased Brewer-Dobson circulation and injection height (Aubry et al., 2021). Other critical mechanisms, such as how future changes in atmospheric circulation and precipitation will affect the volcanic cloud life cycle, remain to be explored (Aubry et al., 2022).

Even if the climatic impact on aerosol diffusion is not considered and the volcanic aerosol evolution after the 1815 Tambora eruption is used to simulate future scenarios, the simulated global cooling and precipitation reduction will be stronger than that in the 1815 climate background affected by enhanced ocean stratification and near-surface circulation (Fasullo et al., 2017). Alternatively, Yang et al. (2022) detected no significant post-Tambora global average climate response between preindustrial and RCP8.5 scenarios because future warming may enhance the sensitivity of monsoon circulation to radiative forcing, causing stronger El Niño-like responses that masks stratification-enhanced ocean cooling. Looking back to volcanic eruptions during both cold and warm periods in paleoclimate records helps us understand the climatic impact of volcanic eruptions under future climate backgrounds.

To better simulate the impact of volcanoes in future scenarios, the simulation capability of stratospheric chemistry and aerosol schemes in climate models, particularly for emission, transport, microphysics, and removal of stratospheric volcanic aerosols, needs to be improved (Zanchettin et al., 2016; Timmreck et al., 2018; Marshall et al., 2022). However, such work has many challenges and abundant computing and storage resources are required for full coupling and long-term simulations when considering the aforementioned processes.

5.2 Changes in daily-intraseasonal variability after volcanic eruptions

Research on the impact of volcanic eruptions on climate is relatively weak in the context of short time scales, particularly within synoptic to intraseasonal time scales. For example, the Hunga Tonga eruption caused global atmospheric waves within a few days. However, it is unknown how this event affected the weather and climate and whether this event can be successfully simulated by atmospheric models (Wright et al., 2022; Zuo et al., 2022). A previous study analyzed the changes in extreme temperature and precipitation after volcanic eruptions using daily data (Zuo et al., 2019), focusing on the interannual time scale rather than the daily-intraseasonal time scales. On the intraseasonal time scale, the Madden-Julian Oscillation (MJO) is a dominant mode over tropical regions; however, whether changes in the air-sea interaction under volcanic forcing will affect the MJO is unclear. Furthermore, local extreme weather events may be induced at the time of the volcanic eruption. Such events can be related to the eruption rate and strength, material proportion, location (i.e., longitude, latitude, and elevation), and season, which are often overlooked. Hence, additional work regarding the layout and analysis of local volcanic monitoring and meteorological observation data is required.

In terms of tropical cyclones (TCs), several scholars have proposed that tropical MVEs can weaken TC activity. After the 1982 and 1991 eruptions, the observed Atlantic hurricane activity was significantly weakened (Evan, 2012). Observations showed the collapse of Typhoon Yunya on June 16, 1991, as it crossed Mount Pinatubo and the record-breaking Jianghuai flood from June 29, 1991, to July 15, 1991 (Ding, 1993; Xing and Liu, 2023). In the North Atlantic, documentary and proxy reconstructions of the past 300 years have shown a weakened frequency of TCs for up to three years after tropical MVEs (Guevara-Murua et al.,

2015). Simulations from the CESM-LME indicated similar results to those of the observation and reconstructions. In contrast, several scholars have proposed that the observed weakened TC activity is not caused by volcanic eruptions (Camargo and Polvani, 2019). The resolution of the current atmospheric model is too coarse (essentially >1°) to accurately account for complex tropical air-sea interactions and describe TC dynamics, making it difficult to analyze the true volcanic impact on TCs. Thus, increasing the model resolution and improving the representation of TC dynamics provide some insights into the potential for future research.

5.3 Volcanic influence on abrupt climate change on a longer time scale

The ability of volcanic forcing to affect the occurrence of abrupt paleoclimate events is of considerable research interest. Supervolcanic eruptions (VEI ⩾7) are considered to be a crucial factor that contributes to abrupt changes in climate. The Toba Volcano erupted at approximately 74 ka BP, with an estimated VEI of 8, approximately two orders of magnitude greater than that of the 1815 Tambora eruption, making it one of the largest eruptions of the Quaternary period. Studies simulating the impact of a Toba-like eruption on the climate and environment revealed the high probability of remarkably reduced temperature and precipitation in Asia and North America (Black et al., 2021). During 73 ka BP, a millennial-scale cold event was recorded simultaneously in the Greenland ice core and Asian stalagmite records (i.e., Greenland Stadial-20 (GS-20) and Chinese Stadial-20 (CS-20)). The CS-20 (74.0–72.5 ka BP) was the weakest Asian monsoon event during the Last Glacial period (Du et al., 2019) and might be related to the Tuba eruption.

The Younger Dryas (YD; approximately 12.8–11.6 ka BP) event was a global-scale abrupt climate change event, with substantial cooling in the NH middle and high latitudes; however, the controlling mechanism of this event remains uncertain. Previous studies reported that the Laacher See eruption occurred immediately before the YD event, indicating a potential volcanic eruption trigger (Baldini et al., 2018). However, the latest chronology shows that the Laacher See eruption occurred at 13.0 ka BP, approximately two centuries earlier than the YD event, which precludes a direct link between the two (Reinig et al., 2021). Abbott et al. (2021) recently highlighted four major bipolar volcanic events and a series of smaller volcanic events during the period of 12.98–12.87 ka BP, particularly in NH. The intensity and duration of these events exceeded the most active historical volcanic periods (i.e., LIA and DACP). Such work showed that clusters of volcanic events need to be considered when exploring the triggering mechanism of the YD event.

6. Summary

(1) Widely used reconstructions of volcanic activity over the past two millennia include Gao2008, Crowley2013, and Sigl2015. The differences in these reconstructions arise from the original ice core data, reconstruction methods, and judgment criteria. Frequent MVEs occurred during cold epochs (i.e., 530–700, 1200–1460, and 1600–1840 CE), whereas quiescent MVE periods characterized warm epochs (i.e., 0–200 and 900–1100 CE). The strongest eruption in China was the Changbaishan eruption in 946 CE; however, it only exhibited a muted climatic response.

(2) The reconstruction and assimilation data showed considerable cooling throughout the globe and China several years after MVEs; however, the magnitude of cooling is not completely consistent with volcanic intensity. In contrast, the cooling simulated by the PMIP models displays a remarkable linear relationship with volcanic intensity. All data indicate the proclivity of interdecadal-scale cold events to occur in NH and China in the events of major and successive moderate volcano eruptions.

(3) The reconstruction, simulation, and assimilation data showed a decrease in global and monsoonal precipitation after MVEs. Over China, increased precipitation occurred over the Yangtze River Basin in response to tropical MVEs; however, divergent responses are observed over north and northeast China and the southern Tibetan Plateau when using different data. Frequent volcanic eruptions, volcanism superimposed on low solar irradiation, and internal variability superimposed on volcanism may cause decadal droughts.

(4) Tree-ring and modeling data showed that an El Niño event occurs after tropical MVEs, which induces the WNPAC and transports moisture to the Yangtze River Basin; however, coral $\delta^{18}O$ records indicate no significant El Niño event. MVEs may contribute to a cold AMO and extend the periodicity of AMO by modulating the sea-ice processes, NAO, and AMOC. After removing the global cooling signal, the volcanic impact on the AMO is weakened, increasing the likelihood of data-model disagreement. Uncertainties in ENSO and AMO responses to MVEs further influence divergent climatic changes in the globe and China, causing model-reconstruction disagreements. The impact of MVEs on other internal variability necessitates further exploration.

(5) Robust understanding of the volcanic impact on regional climate, particularly the modulation role of internal climate variability on hydroclimate, the daily–intraseasonal weather responses, or the abrupt climate change during the Last Glacial period, relies on the dedicated improvement on volcanic forcing reconstruction, stratospheric chemistry–aerosol-climate model development, and the physical mechanism of MVEs affecting climate.

Acknowledgements *We thank the GPCP, PMIP, CESM-LME,*

PHYDA, and LMR for providing the observation, simulation, and assimilation data and thank the researchers who provided the reconstructions. We thank anonymous reviewers for their valuable comments and suggestions. This work was supported by the National Natural Science Foundation of China (Grant Nos. 42130604, 42105044, 41971108, 42111530182 & 41971021), the Consultation and Review Project of Chinese Academy of Sciences (Grant No. 2022-ZW04-A-010), the Swedish STINT (Grant No. CH2019-8377), the Future Earth Global Secretariat Hub China, the International Research Center of Big Data for Sustainable Development Goals (Grant No. CBAS2022GSP08), and the Priority Academic Program Development of Jiangsu Higher Education Institutions (Grant No. 164320H116).

Conflict of interest The authors declare that they have no conflict of interest.

References

Abbott P M, Niemeier U, Timmreck C, Riede F, McConnell J R, Severi M, Fischer H, Svensson A, Toohey M, Reinig F, Sigl M. 2021. Volcanic climate forcing preceding the inception of the Younger Dryas: Implications for tracing the Laacher See eruption. Quat Sci Rev, 274: 107260

Adams B J, Mann M E, Ammann C M. 2003. Proxy evidence for an El Niño-like response to volcanic forcing. Nature, 426: 274–278

Aubry T J, Staunton-Sykes J, Marshall L R, Haywood J, Abraham N L, Schmidt A. 2021. Climate change modulates the stratospheric volcanic sulfate aerosol lifecycle and radiative forcing from tropical eruptions. Nat Commun, 12: 4708

Aubry T J, Farquharson J I, Rowell C R, Watt S F L, Pinel V, Beckett F, Fasullo J, Hopcroft P O, Pyle D M, Schmidt A, Sykes J S. 2022. Impact of climate change on volcanic processes: Current understanding and future challenges. Bull Volcanol, 84: 58

Bai M, Zheng J, Hao Z, Zhang X, Zeng G. 2019. Hydroclimate patterns over the Northern Hemisphere when megadroughts occurred in North China during the last millennium. Clim Change, 157: 365–385

Baldini J U L, Brown R J, Mawdsley N. 2018. Evaluating the link between the sulfur-rich Laacher See volcanic eruption and the Younger Dryas climate anomaly. Clim Past, 14: 969–990

Black B A, Lamarque J F, Marsh D R, Schmidt A, Bardeen C G. 2021. Global climate disruption and regional climate shelters after the Toba supereruption. Proc Natl Acad Sci USA, 118: e2013046118

Booth B B B, Dunstone N J, Halloran P R, Andrews T, Bellouin N. 2019. Aerosols implicated as a prime driver of twentieth-century North Atlantic climate variability. Nature, 484: 228–232

Brohan P, Kennedy J J, Harris I, Tett S F B, Jones P D. 2006. Uncertainty estimates in regional and global observed temperature changes: A new data set from 1850. J Geophys Res, 111: D12106

Brönnimann S, Franke J, Nussbaumer S U, Zumbühl H J, Steiner D, Trachsel M, Hegerl G C, Schurer A, Worni M, Malik A, Flückiger J, Raible C C. 2019. Last phase of the Little Ice Age forced by volcanic eruptions. Nat Geosci, 12: 650–656

Büntgen U, Eggertsson Ó, Wacker L, Sigl M, Ljungqvist F C, Di Cosmo N, Plunkett G, Krusic P J, Newfield T P, Esper J, Lane C, Reinig F, Oppenheimer C. 2017. Multi-proxy dating of Iceland's major pre-settlement Katla eruption to 822–823 CE. Geology, 45: 783–786

Büntgen U, Myglan V S, Ljungqvist F C, McCormick M, Di Cosmo N, Sigl M, Jungclaus J, Wagner S, Krusic P J, Esper J, Kaplan J O, de Vaan M A C, Luterbacher J, Wacker L, Tegel W, Kirdyanov A V. 2016. Cooling and societal change during the Late Antique Little Ice Age from 536 to around 660 AD. Nat Geosci, 9: 231–236

Camargo S J, Polvani L M. 2019. Little evidence of reduced global tropical cyclone activity following recent volcanic eruptions. NPJ Clim Atmos Sci, 2: 14

Chai J, Liu F, Xing C, Wang B, Gao C, Liu J, Chen D. 2020. A robust equatorial Pacific westerly response to tropical volcanism in multiple models. Clim Dyn, 55: 3413–3429

Chen D, Lian T, Fu C, Cane M A, Tang Y, Murtugudde R, Song X, Wu Q, Zhou L. 2015. Strong influence of westerly wind bursts on El Niño diversity. Nat Geosci, 8: 339–345

Chen K, Ning L, Liu Z, Liu J, Yan M, Sun W, Li L, Shi Z. 2022a. Modulating and resetting impacts of different volcanic eruptions on North Atlantic SST variations. J Geophys Res-Atmos, 127: e2021JD036246

Chen K, Ning L, Liu Z, Liu J, Yan M, Sun W, Yuan L, Lv G, Li L, Jin C, Shi Z. 2020. One drought and one volcanic eruption influenced the history of China: The late Ming Dynasty mega-drought. Geophys Res Lett, 47: e2020GL088124

Chen K, Ning L, Liu Z, Liu J, Yan M, Sun W, Yuan L, Lv G, Li L, Jin C, Shi Z. 2022b. Nonlinear responses of droughts over China to volcanic eruptions at different drought phases. Geophys Res Lett, 49: e2021GL096454

Clement A C, Seager R, Cane M A, Zebiak S E. 1996. An ocean dynamical thermostat. J Clim, 9: 2190–2196

Clement A, Bellomo K, Murphy L N, Cane M A, Mauritsen T, Rädel G, Stevens B. 2015. The Atlantic Multidecadal Oscillation without a role for ocean circulation. Science, 350: 320–324

Cole-Dai J, Mosley-Thompson E, Thompson L G. 1997. Annually resolved southern hemisphere volcanic history from two Antarctic ice cores. J Geophys Res, 102: 16761–16771

Crowley T J, Unterman M B. 2013. Technical details concerning development of a 1200 yr proxy index for global volcanism. Earth Syst Sci Data, 5: 187–197

Cook E R, Krusic P J, Anchukaitis K J, Buckley B M, Nakatsuka T, Sano M. 2013. Tree-ring reconstructed summer temperature anomalies for temperate East Asia since 800 C.E.. Clim Dyn, 41: 2957–2972

Dai Z, Wang B, Zhu L, Liu J, Sun W, Li L, Lü G, Ning L, Yan M, Chen K. 2022. Atlantic multidecadal variability response to external forcing during the past two millenniums. J Clim, 35: 8103–8115

Dee S G, Cobb K M, Emile-Geay J, Ault T R, Edwards R L, Cheng H, Charles C D. 2020. No consistent ENSO response to volcanic forcing over the last millennium. Science, 367: 1477–1481

Ding Y. 1993. Research on the 1991 Heavy Precipitation over the Yangtze River (in Chinese). Beijing: China Meteor Press. 255

Du W, Cheng H, Xu Y, Yang X, Zhang P, Sha L, Li H, Zhu X, Zhang M, Stríkis N M, Cruz F W, Edwards R L, Zhang H, Ning Y. 2019. Timing and structure of the weak Asian Monsoon event about 73,000 years ago. Quat Geochronol, 53: 101003

Emile-Geay J, Seager R, Cane M A, Cook E R, Haug G H. 2008. Volcanoes and ENSO over the past millennium. J Clim, 21: 3134–3148

Evan A T. 2012. Atlantic hurricane activity following two major volcanic eruptions. J Geophys Res, 117: D06101

Fasullo J T, Tomas R, Stevenson S, Otto-Bliesner B, Brady E, Wahl E. 2017. The amplifying influence of increased ocean stratification on a future year without a summer. Nat Commun, 8: 1

Feng S, Hu Q, Wu Q, Mann M E. 2013. A gridded reconstruction of warm season precipitation for Asia spanning the past half millennium. J Clim, 26: 2192–2204

Fujiwara M, Martineau P, Wright J S. 2020. Surface temperature response to the major volcanic eruptions in multiple reanalysis data sets. Atmos Chem Phys, 20: 345–374

Gao Y, Gao C C. 2021. Differences in three sets of volcanic forcing data and their impacts on climate model simulation (in Chinese). Clim Change Res, 17: 305–316

Gao C C, Gao Y J. 2018. Revisited Asian monsoon hydroclimate response to volcanic eruptions. J Geophys Res-Atmos, 123: 7883–7896

Gao C, Gao Y, Zhang Q, Shi C. 2017. Climatic aftermath of the 1815 Tambora eruption in China. J Meteorol Res, 31: 28–38

Gao C, Ludlow F, Matthews J A, Stine A R, Robock A, Pan Y, Breen R, Nolan B, Sigl M. 2021. Volcanic climate impacts can act as ultimate and proximate causes of Chinese dynastic collapse. Commun Earth Environ, 2: 234

Gao C, Robock A, Ammann C. 2008. Volcanic forcing of climate over the last 1500 years: An improved ice-core based index for climate models. J Geophys Res, 114: D2311
Ge Q, Hao Z, Zheng J, Shao X. 2013. Temperature changes over the past 2000 yr in China and comparison with the Northern Hemisphere. Clim Past, 9: 1153–1160
Guevara-Murua A, Hendy E J, Rust A C, Cashman K V. 2015. Consistent decrease in North Atlantic Tropical Cyclone frequency following major volcanic eruptions in the last three centuries. Geophys Res Lett, 42: 9425–9432
Hao Z, Xiong D, Zheng J, Yang L E, Ge Q. 2020. Volcanic eruptions, successive poor harvests and social resilience over southwest China during the 18–19th century. Environ Res Lett, 15: 105011
Hartmann D L. 2022. The Antarctic ozone hole and the pattern effect on climate sensitivity. Proc Natl Acad Sci USA, 119: e2207889119
Iacovino K, Ju-Song K, Sisson T, Lowenstern J, Kuk-Hun R, Jong-Nam J, Kun-Ho S, Song-Hwan H, Oppenheimer C, Hammond J O S, Donovan A, Liu K W, Kum-Ran R. 2016. Quantifying gas emissions from the "Millennium Eruption" of Paektu volcano, Democratic People's Republic of Korea/China. Sci Adv, 2: e1600913
IPCC. 2021. Summary for Policymakers. In: Climate Change 2021: The Physical Science Basis. Contribution of Working Group I to the Sixth Assessment Report of the Intergovernmental Panel on Climate Change. In: Masson-Delmotte V, P Zhai, A Pirani, S L Connors, C Péan, S Berger, N Caud, Y Chen, L Goldfarb, M I Gomis, M Huang, K Leitzell, E Lonnoy, J B R Matthews, T K Maycock, T Waterfield, O Yelekçi, R Yu and B Zhou, eds. Cambridge University Press
Iles C E, Hegerl G C, Schurer A P, Zhang X. 2013. The effect of volcanic eruptions on global precipitation. J Geophys Res-Atmos, 118: 8770–8786
Iwi A M, Hermanson L, Haines K, Sutton R T. 2012. Mechanisms linking volcanic aerosols to the Atlantic meridional overturning circulation. J Clim, 25: 3039–3051
Jungclaus J H, Bard E, Baroni M, Braconnot P, Cao J, Chini L P, Egorova T, Evans M, González-Rouco J F, Goosse H, Hurtt G C, Joos F, Kaplan J O, Khodri M, Klein Goldewijk K, Krivova N, LeGrande A N, Lorenz S J, Luterbacher J, Man W, Maycock A C, Meinshausen M, Moberg A, Muscheler R, Nehrbass-Ahles C, Otto-Bliesner B I, Phipps S J, Pongratz J, Rozanov E, Schmidt G A, Schmidt H, Schmutz W, Schurer A, Shapiro A I, Sigl M, Smerdon J E, Solanki S K, Timmreck C, Toohey M, Usoskin I G, Wagner S, Wu C J, Yeo K L, Zanchettin D, Zhang Q, Zorita E. 2017. The PMIP4 contribution to CMIP6—Part 3: The last millennium, scientific objective, and experimental design for the PMIP4 past1000 simulations. Geosci Model Dev, 10: 4005–4033
Khodri M, Izumo T, Vialard J, Janicot S, Cassou C, Lengaigne M, Mignot J, Gastineau G, Guilyardi E, Lebas N, Robock A, McPhaden M J. 2017. Tropical explosive volcanic eruptions can trigger El Niño by cooling tropical Africa. Nat Commun, 8: 778
Knudsen M F, Jacobsen B H, Seidenkrantz M S, Olsen J. 2014. Evidence for external forcing of the Atlantic Multidecadal Oscillation since termination of the Little Ice Age. Nat Commun, 5: 3323
Lapointe F, Bradley R S, Francus P, Balascio N L, Abbott M B, Stoner J S, St-Onge G, De Coninck A, Labarre T. 2020. Annually resolved Atlantic sea surface temperature variability over the past 2,900 y. Proc Natl Acad Sci USA, 117: 27171–27178
Lavigne F, Degeai J P, Komorowski J C, Guillet S, Robert V, Lahitte P, Oppenheimer C, Stoffel M, Vidal C M, Surono C M, Pratomo I, Wassmer P, Hajdas I, Hadmoko D S, de Belizal E. 2013. Source of the great A.D. 1257 mystery eruption unveiled, Samalas volcano, Rinjani Volcanic Complex, Indonesia. Proc Natl Acad Sci USA, 110: 16742–16747
Li J, Xie S P, Cook E R, Morales M S, Christie D A, Johnson N C, Chen F, D'Arrigo R, Fowler A M, Gou X, Fang K. 2013. El Niño modulations over the past seven centuries. Nat Clim Change, 3: 822–826
Liu B, Wang B, Liu J, Chen D, Ning L, Yan M, Sun W, Chen K. 2020. Global and polar region temperature change induced by single mega volcanic eruption based on community earth system model simulation. Geophys Res Lett, 47: e2020GL089416
Liu F, Chai J, Wang B, Liu J, Zhang X, Wang Z. 2016. Global monsoon precipitation responses to large volcanic eruptions. Sci Rep, 6: 24331
Liu F, Gao C, Chai J, Robock A, Wang B, Li J, Zhang X, Huang G, Dong W. 2022a. Tropical volcanism enhanced the East Asian summer monsoon during the last millennium. Nat Commun, 13: 3429
Liu F, Li J, Wang B, Liu J, Li T, Huang G, Wang Z. 2018a. Divergent El Niño responses to volcanic eruptions at different latitudes over the past millennium. Clim Dyn, 50: 3799–3812
Liu F, Zhao T, Wang B, Liu J, Luo W. 2018b. Different global precipitation responses to solar, volcanic, and greenhouse gas forcings. J Geophys Res-Atmos, 123: 4060–4072
Liu F, Xing C, Chen L, Gao C, Lian T, Zhou S, Wang H, Wang B, Dong W. 2022b. Relative roles of land and ocean cooling in triggering an El Niño following tropical volcanic eruptions. Geophys Res Lett, 49: e2022GL100609
Ljungqvist F C, Zhang Q, Brattström G, Krusic P J, Seim A, Li Q, Zhang Q, Moberg A. 2019. Centennial-scale temperature change in last millennium simulations and proxy-based reconstructions. J Clim, 32: 2441–2482
Luterbacher J, Pfister C. 2015. The year without a summer. Nat Geosci, 8: 246–248
Man W, Zhou T, Jungclaus J H. 2014. Effects of large volcanic eruptions on global summer climate and East Asian monsoon changes during the last millennium: Analysis of MPI-ESM simulations. J Clim, 27: 7394–7409
Mann M E, Fuentes J D, Rutherford S. 2012. Underestimation of volcanic cooling in tree-ring-based reconstructions of hemispheric temperatures. Nat Geosci, 5: 202–205
Mann M E, Steinman B A, Brouillette D J, Miller S K. 2021. Multidecadal climate oscillations during the past millennium driven by volcanic forcing. Science, 371: 1014–1019
Mann M E, Zhang Z, Rutherford S, Bradley R S, Hughes M K, Shindell D, Ammann C, Faluvegi G, Ni F. 2009. Global signatures and dynamical origins of the little ice age and medieval climate anomaly. Science, 326: 1256–1260
Marshall L R, Maters E C, Schmidt A, Timmreck C, Robock A, Toohey M. 2022. Volcanic effects on climate: recent advances and future avenues. Bull Volcanol, 84: 54
McGregor S, Timmermann A. 2011. The effect of explosive tropical volcanism on ENSO. J Clim, 24: 2178–2191
Michel S L L, Swingedouw D, Ortega P, Gastineau G, Mignot J, McCarthy G, Khodri M. 2022. Early warning signal for a tipping point suggested by a millennial Atlantic Multidecadal Variability reconstruction. Nat Commun, 13: 5176
Millán L, Santee M L, Lambert A, Livesey N J, Werner F, Schwartz M J, Pumphrey H C, Manney G L, Wang Y, Su H, Wu L, Read W G, Froidevaux L. 2022. The Hunga Tonga-Hunga Ha'apai hydration of the stratosphere. Geophys Res Lett, 49: e2022GL099381
Miller G H, Geirsdóttir Á, Zhong Y, Larsen D J, Otto-Bliesner B L, Holland M M, Bailey D A, Refsnider K A, Lehman S J, Southon J R, Anderson C, Björnsson H, Thordarson T. 2012. Abrupt onset of the Little Ice Age triggered by volcanism and sustained by sea-ice/ocean feedbacks. Geophys Res Lett, 39: 1–5
Neukom R, Barboza L, Erb M, Shi F, Emile-Geay J, Evans M, Franke J, Kaufman D, Lücke L, Rehfeld K, Schurer A, Zhu F, Brönnimann S, Hakim G, Henley B, Ljungqvist F, McKay N, Valler V, Gunten L. 2019. Consistent multidecadal variability in global temperature reconstructions and simulations over the Common Era. Nat Geosci, 12: 643–649, doi: 10.1038/s41561-019-0400-0
Ning L, Chen K, Liu J, Liu Z, Yan M, Sun W, Jin C, Shi Z. 2020. How do volcanic eruptions influence decadal megadroughts over Eastern China? J Clim, 33: 8195–8207
Ning L, Liu J, Bradley R S, Yan M, Chen K, Sun W, Jin C. 2019. Elevation-dependent cooling caused by volcanic eruptions during the last millennium. Intl J Clim, 40: 3142–3149
Ning L, Liu J, Sun W. 2017. Influences of volcano eruptions on Asian

summer monsoon over the last 110 years. Sci Rep, 7: 42626
Ohba M, Shiogama H, Yokohata T, Watanabe M. 2013. Impact of strong tropical volcanic eruptions on ENSO simulated in a coupled GCM. J Clim, 26: 5169–5182
Oppenheimer C, Wacker L, Xu J, Galván J D, Stoffel M, Guillet S, Corona C, Sigl M, Di Cosmo N, Hajdas I, Pan B, Breuker R, Schneider L, Esper J, Fei J, Hammond J O S, Büntgen U. 2017. Multi-proxy dating the 'Millennium Eruption' of Changbaishan to late 946 CE. Quat Sci Rev, 158: 164–171
Ortega P, Lehner F, Swingedouw D, Masson-Delmotte V, Raible C C, Casado M, Yiou P. 2015. A model-tested North Atlantic Oscillation reconstruction for the past millennium. Nature, 523: 71–74
Otterå O H, Bentsen M, Drange H, Suo L. 2010. External forcing as a metronome for Atlantic multidecadal variability. Nat Geosci, 3: 688–694
Otto-Bliesner B L, Brady E C, Fasullo J, Jahn A, Landrum L, Stevenson S, Rosenbloom N, Mai A, Strand G. 2016. Climate variability and change since 850 CE: An ensemble approach with the Community Earth System Model. Bull Am Meteorol Soc, 97: 735–754
Paik S, Min S K. 2017. Climate responses to volcanic eruptions assessed from observations and CMIP5 multi-models. Clim Dyn, 48: 1017–1030
Paik S, Min S K, Iles C E, Fischer E M, Schurer A P. 2020. Volcanic-induced global monsoon drying modulated by diverse El Niño responses. Sci Adv, 6: eaba1212
Peng Y, Shen C, Wang W C, Xu Y. 2010. Response of summer precipitation over eastern China to large volcanic eruptions. J Clim, 23: 818–824
Proud S R, Prata A T, Schmauß S. 2022. The January 2022 eruption of Hunga Tonga-Hunga Ha'apai volcano reached the mesosphere. Science, 378: 554–557
Reinig F, Wacker L, Jöris O, Oppenheimer C, Guidobaldi G, Nievergelt D, Adolphi F, Cherubini P, Engels S, Esper J, Land A, Lane C, Pfanz H, Remmele S, Sigl M, Sookdeo A, Büntgen U. 2021. Precise date for the Laacher See eruption synchronizes the Younger Dryas. Nature, 595: 66–69
Robock A. 2000. Volcanic eruptions and climate. Rev Geophys, 38: 191–219
Robock A. 2020. Comment on "No consistent ENSO response to volcanic forcing over the last millennium". Science, 369: 6509
Schmidt A, Carslaw K S, Mann G W, Wilson M, Breider T J, Pickering S J, Thordarson T. 2010. The impact of the 1783–1784 AD Laki eruption on global aerosol formation processes and cloud condensation nuclei. Atmos Chem Phys, 10: 6025–6041
Schneider D P, Ammann C M, Otto-Bliesner B L, Kaufman D S. 2009. Climate response to large, high-latitude and low-latitude volcanic eruptions in the Community Climate System Model. J Geophys Res, 114: D15101
Schneider L, Smerdon J E, Pretis F, Hartl-Meier C, Esper J. 2017. A new archive of large volcanic events over the past millennium derived from reconstructed summer temperatures. Environ Res Lett, 12: 119501
Schneider U, Becker A, Finger P, Meyer-Christoffer A, Ziese M, Rudolf B. 2014. GPCC's new land surface precipitation climatology based on quality-controlled in situ data and its role in quantifying the global water cycle. Theor Appl Climatol, 115: 15–40
Shen T, Sun W, Liu J, Wang B, Chen D, Ning L, Chen K. 2022. Secular changes of the decadal relationship between the Northern Hemisphere land monsoon rainfall and sea surface temperature over the past millennium in climate model simulations. J Geophys Res-Atmos, 127: e2022JD037065
Shi F, Ge Q, Yang B, Li J, Yang F, Ljungqvist F C, Solomina O, Nakatsuka T, Wang N, Zhao S, Xu C, Fang K, Sano M, Chu G, Fan Z, Gaire N P, Zafar M U. 2015. A multi-proxy reconstruction of spatial and temporal variations in Asian summer temperatures over the last millennium. Clim Change, 131: 663–676
Shi F, Yang B, Von Gunten L. 2012. Preliminary multiproxy surface air temperature field reconstruction for China over the past millennium. Sci China Earth Sci, 55: 2058–2067
Shi F, Zhao S, Guo Z, Goosse H, Yin Q. 2017. Multi-proxy reconstructions of May–September precipitation field in China over the past 500 years. Clim Past, 13: 1919–1938
Shi H, Wang B, Cook E R, Liu J, Liu F. 2018. Asian summer precipitation over the past 544 years reconstructed by merging tree rings and historical documentary records. J Clim, 31: 7845–7861
Sigl M, Winstrup M, McConnell J R, Welten K C, Plunkett G, Ludlow F, Büntgen U, Caffee M, Chellman N, Dahl-Jensen D, Fischer H, Kipfstuhl S, Kostick C, Maselli O J, Mekhaldi F, Mulvaney R, Muscheler R, Pasteris D R, Pilcher J R, Salzer M, Schüpbach S, Steffensen J P, Vinther B M, Woodruff T E. 2015. Timing and climate forcing of volcanic eruptions for the past 2,500 years. Nature, 523: 543–549
Sigl M, Toohey M, McConnell J R, Cole-Dai J, Severi M. 2022. Volcanic stratospheric sulfur injections and aerosol optical depth during the Holocene (past 11 500 years) from a bipolar ice-core array. Earth Syst Sci Data, 14: 3167–3196
Singh M, Krishnan R, Goswami B, Choudhury A D, Swapna P, Vellore R, Prajeesh A G, Sandeep N, Venkataraman C, Donner R V, Marwan N, Kurths J. 2020. Fingerprint of volcanic forcing on the ENSO-Indian monsoon coupling. Sci Adv, 6: eaba8164
Slawinska J, Robock A. 2018. Impact of volcanic eruptions on decadal to centennial fluctuations of Arctic sea ice extent during the last millennium and on initiation of the little ice age. J Clim, 31: 2145–2167
Smith V C, Costa A, Aguirre-Díaz G, Pedrazzi D, Scifo A, Plunkett G, Poret M, Tournigand P Y, Miles D, Dee M W, McConnell J R, Sunyé-Puchol I, Harris P D, Sigl M, Pilcher J R, Chellman N, Gutiérrez E. 2020. The magnitude and impact of the 431 CE Tierra Blanca Joven eruption of Ilopango, El Salvador. Proc Natl Acad Sci USA, 117: 26061–26068
Steiger N J, Smerdon J E, Cook E R, Cook B I. 2018. A reconstruction of global hydroclimate and dynamical variables over the Common Era. Sci Data, 5: 180086
Stevenson S, Fasullo J T, Otto-Bliesner B L, Tomas R A, Gao C. 2017. Role of eruption season in reconciling model and proxy responses to tropical volcanism. Proc Natl Acad Sci USA, 114: 1822–1826
Stevenson S, Overpeck J T, Fasullo J, Coats S, Parsons L, Otto-Bliesner B, Ault T, Loope G, Cole J. 2018. Climate variability, volcanic forcing, and last millennium hydroclimate extremes. J Clim, 31: 4309–4327
Stoffel M, Khodri M, Corona C, Guillet S, Poulain V, Bekki S, Guiot J, Luckman B H, Oppenheimer C, Lebas N, Beniston M, Masson-Delmotte V. 2015. Estimates of volcanic-induced cooling in the Northern Hemisphere over the past 1,500 years. Nat Geosci, 8: 784–788
Sun W, Liu J, Gao C, Chen M. 2021. Response of temperature in different latitudes of the Northern Hemisphere to volcanic eruptions during the past 2000 years. Chin Sci Bull, 66: 3194–3204
Sun W, Liu J, Wang B, Chen D, Gao C. 2022. Pacific multidecadal (50–70 year) variability instigated by volcanic forcing during the Little Ice Age (1250–1850). Clim Dyn, 59: 231–244
Sun W, Liu J, Wang B, Chen D, Liu F, Wang Z, Ning L, Chen M. 2019a. A "La Niña-like" state occurring in the second year after large tropical volcanic eruptions during the past 1500 years. Clim Dyn, 52: 7495–7509
Sun W, Wang B, Liu J, Chen D, Gao C, Ning L, Chen L. 2019b. How Northern high-latitude volcanic eruptions in different seasons affect ENSO? J Clim, 32: 3245–3262
Tardif R, Hakim G J, Perkins W A, Horlick K A, Erb M P, Emile-Geay J, Anderson D M, Steig E J, Noone D. 2019. Last Millennium Reanalysis with an expanded proxy database and seasonal proxy modeling. Clim Past, 15: 1251–1273
Tejedor E, Steiger N J, Smerdon J E, Serrano-Notivoli R, Vuille M. 2021. Global hydroclimatic response to tropical volcanic eruptions over the last millennium. Proc Natl Acad Sci USA, 118: e2019145118
Timmreck C, Mann G W, Aquila V, Hommel R, Lee L A, Schmidt A, Brühl C, Carn S, Chin M, Dhomse S S, Diehl T, English J M, Mills M J, Neely R, Sheng J, Toohey M, Weisenstein D. 2018. The Interactive Stratospheric Aerosol Model Intercomparison Project (ISA-MIP): Motivation and experimental design. Geosci Model Dev, 11: 2581–2608

Toohey M, Sigl M. 2017. Volcanic stratospheric sulfur injections and aerosol optical depth from 500 BCE to 1900 CE. Earth Syst Sci Data, 9: 809–831
Wang B, Wu R, Fu X. 2000. Pacific-East Asian teleconnection: How does ENSO affect East Asian climate? J Clim, 13: 1517–1536
Wang J, Yang B, Ljungqvist F C, Luterbacher J, Osborn T J, Briffa K R, Zorita E. 2017. Internal and external forcing of multidecadal Atlantic climate variability over the past 1,200 years. Nat Geosci, 10: 512–517
Wei H, Liu G, Gill J. 2013. Review of eruptive activity at Tianchi volcano, Changbaishan, northeast China: implications for possible future eruptions. Bull Volcanol, 75: 706
Wright C J, Hindley N P, Alexander M J, Barlow M, Hoffmann L, Mitchell C N, Prata F, Bouillon M, Carstens J, Clerbaux C, Osprey S M, Powell N, Randall C E, Yue J. 2022. Surface-to-space atmospheric waves from Hunga Tonga–Hunga Ha'apai eruption. Nature, 609: 741–746
Xing C, Liu F. 2023. Mount Pinatubo eruption caused the major East China flood in 1991. Innov Geosci, 1: 100032
Xing C, Liu F, Wang B, Chen D, Liu J, Liu B. 2020. Boreal winter surface air temperature responses to large tropical volcanic Eruptions in CMIP5 models. J Clim, 33: 2407–2426
Yang L, Gao Y, Gao C, Liu F. 2022. Climate responses to tambora-size volcanic eruption and the impact of warming climate. Geophys Res Lett, 49: e2021GL097477
Zanchettin D, Khodri M, Timmreck C, Toohey M, Schmidt A, Gerber E P, Hegerl G, Robock A, Pausata F S R, Ball W T, Bauer S E, Bekki S, Dhomse S S, LeGrande A N, Mann G W, Marshall L, Mills M, Marchand M, Niemeier U, Poulain V, Rozanov E, Rubino A, Stenke A, Tsigaridis K, Tummon F. 2016. The Model Intercomparison Project on the climatic response to Volcanic forcing (VolMIP): experimental design and forcing input data for CMIP6. Geosci Model Dev, 9: 2701–2719
Zanchettin D, Timmreck C, Graf H F, Rubino A, Lorenz S, Lohmann K, Krüger K, Jungclaus J H. 2012. Bi-decadal variability excited in the coupled ocean–atmosphere system by strong tropical volcanic eruptions. Clim Dyn, 39: 419–444
Zhang H, Werner J P, García-Bustamante E, González-Rouco F, Wagner S, Zorita E, Fraedrich K, Jungclaus J H, Ljungqvist F C, Zhu X, Xoplaki E, Chen F, Duan J, Ge Q, Hao Z, Ivanov M, Schneider L, Talento S, Wang J, Yang B, Luterbacher J. 2018. East Asian warm season temperature variations over the past two millennia. Sci Rep, 8: 7702
Zhang R, Sumi A, Kimoto M. 1996. Impact of El Niño on the East Asian Monsoon. J Meteorol Soc Jpn, 74: 49–62
Zhang R, Sutton R, Danabasoglu G, Kwon Y, Marsh R, Yeager S G, Amrhein D E, Little C M. 2019. A review of the role of the Atlantic Meridional Overturning Circulation in Atlantic Multidecadal Variability and associated climate impacts. Rev Geophys, 57: 316–375
Zheng J, Wang W C, Ge Q, Man Z, Zhang P. 2006. Precipitation variability and extreme events in eastern China during the past 1500 years. Terr Atmos Ocean Sci, 17: 579
Zhong Y, Miller G H, Otto-Bliesner B L, Holland M M, Bailey D A, Schneider D P, Geirsdottir A. 2010. Centennial-scale climate change from decadally-paced explosive volcanism: A coupled Sea ice-ocean mechanism. Clim Dyn, 37: 2373–2387
Zhu F, Emile-Geay J, Anchukaitis K J, Hakim G J, Wittenberg A T, Morales M S, Toohey M, King J. 2022. A re-appraisal of the ENSO response to volcanism with paleoclimate data assimilation. Nat Commun, 13: 747
Zuo M, Zhou T, Man W. 2019. Hydroclimate responses over global monsoon regions following volcanic eruptions at different latitudes. J Clim, 32: 4367–4385
Zuo M, Zhou T, Man W, Chen X, Liu J, Liu F, Gao C. 2022. Volcanoes and climate: Sizing up the impact of the recent Hunga Tonga-Hunga Ha'apai Volcanic eruption from a historical perspective. Adv Atmos Sci, 39: 1986–1993
Zhu Y, Bardeen C G, Tilmes S, Mills M J, Wang X, Harvey V L, Taha G, Kinnison D, Portmann R W, Yu P, Rosenlof K H, Avery M, Kloss C, Li C, Glanville A S, Millán L, Deshler T, Krotkov N, Toon O B. 2022. Perturbations in stratospheric aerosol evolution due to the water-rich plume of the 2022 Hunga-Tonga eruption. Commun Earth Environ, 3: 248

(Editorial handling: Dake CHEN)